Title: Online Measurement of the Size Distribution of Pneumatically Conveyed Particles Through Acoustic Emission Detection and Triboelectric Sensing

Authors: Ge Zheng[a]

Yong Yan[b] (Corresponding author)

Yonghui Hu[a]

Wenbiao Zhang[a]

Addresses: [a] School of Control and Computer Engineering

North China Electric Power University, Beijing 102206, China

[b] School of Engineering and Digital Arts

University of Kent, Canterbury, Kent CT2 7NT, U.K.

Tel: 00441227823015

Fax: 00441227456084

Email: y.yan@kent.ac.uk

ABSTRACT

In a thermal power plant online measurement of the size distribution of pneumatically conveyed pulverized fuel is essential for the improvement of combustion efficiency and the reduction of pollutant emissions. In this paper, an innovative instrumentation system based on acoustic emission (AE) detection and triboelectric sensing is proposed for the on-line continuous measurement of particle size distribution. With a waveguide protruding into the flow, the AE signal is generated from the impacts of particles with the waveguide. The peak voltage of the AE signal is related to the particle size and impact velocity. For the first time, two triboelectric sensor arrays each with three arc-shaped electrodes near to the waveguide are used to measure the impact velocity. Meanwhile, a novel particle sizing algorithm with Gaussian prediction is proposed to reduce the effect of overlapping impacts and environmental noise on the peak distribution. With the known impact velocity measured from the triboelectric sensor arrays and the modified peak distribution, the measurement of particle size distribution is achieved. Experimental tests were conducted on a gas–solids two-phase flow rig to assess the performance of the developed measurement system. Silica sands in three size ranges of 116–750 μm, 61–395 μm and 10–246 μm, respectively, were used as test particles. The experimental results demonstrate that Spearman's rank correlation coefficient between the measured and reference size distributions for all test particles is all greater than 0.8, while the discrepancy for each particle size segment is within ±4.8%.

Index Terms– Particle flow, particle size distribution, acoustic emission, triboelectric sensor

I. INTRODUCTION

Size distribution is an important physical characteristic of particles in many industrial processes. During power generation pulverized coal is transported from pulverizing mills to burners through a network of pneumatic conveying pipelines. Online measurement of the size distribution of pneumatically conveyed particles is important for smooth fuel delivery and optimized combustion processes [1, 2]. On the one hand, the presence of large particles in the pipelines will cause unbalanced distribution of fuel to burners, leading to excessive NO_x emission, flame oscillation, slagging, etc. Meanwhile, since it takes longer to burn out larger particles, the chance of incomplete combustion will increase, which reduces the boiler efficiency. On the other hand, it is also uneconomical with the pulverizing system to produce unnecessarily fine particles. Furthermore, excessively small particles will increase the risk of explosion due to spontaneous combustion.

Current practice in the particle sizing of pulverized fuel is performed off-line, usually through isokinetic sampling and sieving [3]. For years, various on-line measurement techniques have been proposed to realize particle sizing, including laser diffraction, digital imaging, electrostatic sensing, microwave scattering and acoustic emission detection [4–8]. However, as the particle flow in a pneumatic pipeline is very complex in terms of gas-solids two-phase flow nature, such as inhomogeneous particle distributions, irregular velocity profiles, variable particle size and shape distributions, moisture content and etc., the particle flow measurement is recognized as a long-standing industrial problem [9, 10]. Due to the inherent complexity of gas-solids two-phase flow in a duct, harsh environmental conditions and high installation and maintenance costs, there have been very few on-line particle sizing instruments currently operating in industry.

Acoustic emission (AE) is the phenomenon of radiation of transient elastic stress waves in solids that occurs when the energy from localized sources within a material rapidly releases. As AE

method is insensitive to environmental conditions with high sensitivity and cost-effectiveness, it is considered as a promising approach to online measurement of the size distribution of pneumatically conveyed particles. Particle size information is deduced through the analysis of the signal due to the impact of particles with the acoustic waveguide. The typical AE signal from a single particle impact and overlapping impacts and the parameters commonly used for analysis are illustrated in Fig. 1. The description of the parameters is given below.

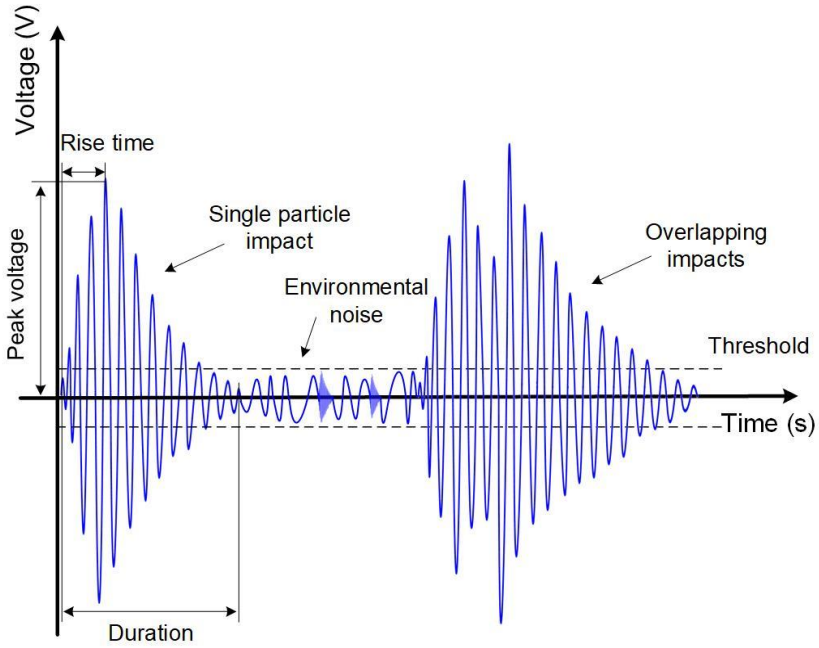

Fig. 1 Typical AE signals and definitions of the key parameters.

Preliminary research by Buttle *et al*. [11] demonstrated the relationship of the peak voltage and rise time of the AE signal with the particle size through theoretical analysis. Practical experiments were conducted on a free-ball particle drop rig with an AE sensor attached on a target plate. From a series of experiments on a slurry impingement erosion test rig, Droubi *et al.* [12] observed that the AE energy was proportional to the mean particle diameter (d) cubed, i.e. d^3. Coghill [13] designed a portable impact size monitor to intermittently measure the particle size of pneumatically conveyed particles. In their work a built-in AE sensor masked by a metal cap with a 2 mm diameter hole was temporally inserted to the flow line. As stated by Coghill, particles smaller than 50 μm

will deviate from striking the impact probe at typical transport velocities of 25 m/s and cannot produce effective AE signals. As shown in Fig. 1, the duration of an AE signal, as a key parameter in their study, is susceptible to interference from overlapping impacts, which will give spurious measurements. The lack of information about the particle impact velocity will also adversely affect the measurement accuracy. Moreover, the mask is easily blocked by particles and hence regular maintenance is required. Therefore, the impact size monitor is not suitable for long-term, routine, online, continuous measurement of particle size distribution. Uher *et al*. [14] established an analytical model describing the relationship between the particle size, velocity and AE signal based on the Hertz theory of impact. The Hertz theory of impact is a classical theory, which assumes that the contact is perfectly elastic during the impact. The test rig consisted of a hopper for solid particles placed over a retention dish, where the variation in particle impact velocity was achieved by varying the height of the hopper.

Zhang *et al*. [15] focused on the study of single particle impacts to reveal the AE sensing mechanism. In consideration of plastic deformation, the Stronge impact theory was applied to describe the particle impact process. Meanwhile, a new model of the relationship between AE signal and particle size was established based on the theory. The experiments were conducted on a single-particle test rig with glass beads to validate this model. Individual glass beads were injected through a small metal rings to obtain the impact velocity which is required in the analysis. However, the particle flow in pneumatic pipelines is very complex, the model cannot be directly used for online size measurement of particles in pneumatic pipelines. Hu *et al.* [8] developed an algorithm for the detection of AE peak voltage. Compared to peak detection algorithms based on maximum search and threshold, the algorithm based on the smoothed local energy is more effective to reduce false detection due to noise corruption to the signal and overlapping of the ringing.

However, for signal peaks due to simultaneous impacts of multiple particles and those submerged in background noise, the peak detection algorithm is no longer effective. Under a range of test conditions, the maximum deviation of the sizing results for the particles of the same-size exceeds 25%. Meanwhile, the maximum discrepancy between the measured and reference size also exceeds 25%. So the accuracy and repeatability of the particle sizing system are unsatisfactory.

Particle impact velocity is the local particle velocity at which the particles collide with the waveguide, which is a key parameter that needs to be measured in on-line particle sizing. The relationship between the AE signal (peak voltage), particle impact velocity and particle size is described in Section II.B. However, measurement of particle velocity is also a challenging problem in pulverized fuel fired power plants [16], not to mention particle impact velocity. In some studies, conveying air velocity as an easily available parameter was often used instead of particle velocity or particle impact velocity [17]. For gas–solid two-phase flow, there is a slip velocity between the solids and gas phases. The relative deviation between the air velocity and the particle velocity across the entire pipe section is usually greater than 5% [18].

Triboelectric phenomenon exists widely in our daily lives or industrial activities [19, 20]. The transportation of particles in a pipe generates triboelectric charges on the particles due to inter-particle interactions, particle-air frictions and particle-wall collisions [9]. For the particle velocity measurement, triboelectric sensing is regarded as the most cost-effective method [9, 16]. Hu *et al*. [8] and Zhang *et al.* [15] used a set of ring-shaped electrodes to measure the particle impact velocity. As its sensing area covers the whole cross sectional area of the pipe, a pair of ring-shaped electrodes can only measure the circumferentially averaged particle velocity across the entire pipe section. However, the impacting area of the AE probe occupies only a very small fraction of the pipe cross section. In view of the complex nature of particle flow in a pneumatic conveying

pipeline, in particular, inhomogeneous particle distribution and irregular velocity profile [9], the circumferentially averaged particle velocity is different from the particle impact velocity which is local to the waveguide. Therefore, the use of air velocity or circumferentially averaged particle velocity as the particle impact velocity will introduce significant errors in particle size measurement.

As shown in Fig. 1, overlapping impacts mean that when the AE pulse generated by the impact of the previous particle has not completely attenuated, another AE pulse is produced. There must be cases where two or more particles impact on the waveguide simultaneously, causing several AE pulses to overlap. When the impacting time intervals of two or more particles are very small, or the signal amplitude of the second particle is too low to submerge in the attenuation signal of the previous one, it is impractical to distinguish the peak voltage of each impact event. For very small particles or those with a low impact velocity, AE pulses are submerged in the environmental noise, so the impact events may be missed. Due to overlapping impacts and environmental noise, the detected peak distribution is different from the expected peak distribution, which will affect the measurement accuracy of particle size distribution.

In summary, despite the various advances in recent years, on-line particle size measurement through AE sensing is still in its early stage of development and many problems remain to be resolved. For instance, it is difficult to identify the peak, duration or rise time of an AE signal when the signals of two particles overlapped. The particle impact velocity is another important factor that affects the AE signal, while the actual velocity of particles that impact the waveguide is difficult to obtain. Moreover, as pulverized fuel particles are rarely spherical, the relationship between the AE signal characteristics and the impact velocity and particle size for spherical particles [8, 14, 15] should not be directly applicable to irregular shaped particles.

In order to overcome the challenges mentioned above, this paper presents a novel instrumentation system for the online measurement of size distribution through AE detection and triboelectric sensing. A waveguide protrudes into the particle flow to generate the AE signal through particle impacts. The peak voltage of the AE pulse contains the information about the impact particles such as the particle size and impact velocity. The novel contribution of this paper includes the following two folds. Firstly, two sets of arc-shaped triboelectric sensor arrays next to the waveguide are used for the first time to measure the impact velocity of particles close to the waveguide. Arc-shaped electrodes are suitable for the measurement of local particle velocities as they are sensitive to particles in its vicinity [9], which is more representative of the particle impact velocity than that from the ring-shaped electrodes. Secondly, the Gaussian model is used for the first time to predict peak distribution generated by large and small particles in order to reduce the deviation between the detected peak distribution and expected distribution due to overlapping impacts and environmental noise. The relationship between the peak AE voltage, impact velocity and particle size, which was established for spherical particles, should be extended for irregular shaped (non-spherical) particles through experimental calibration. With the particle impact velocity obtained from triboelectric sensor arrays and the modified peak distribution, the measurement of particle size distribution is achieved.

II. METHODOLOGY

A. Sensing Arrangement and Sensor Design

When solid particles impact on a plate, transient elastic stress waves are generated and propagate away from the impact points. The AE signal signatures are closely related to the impulsive forces that the particles impose on the plate. The impact force is dependent on particle characteristics,

especially particle size and impact velocity.

The sensing head is composed of an AE probe and three triboelectric sensor arrays each with three arc-shaped electrodes (Fig. 2). An intruded waveguide is employed for both generation and transmission of the elastic stress waves due to the impact of particles. In view of the wear and tear of the waveguide due to the impact by particles, it is made of a wear-resistant material, zirconia ceramic. As shown in Fig. 3, the inside section of the waveguide is semi-cylindrical with a diameter of 10 mm. The flat surface faces the direction of the flow, allowing normal impact of particles with the waveguide. The thickness of the inside section of the waveguide is 5 mm. In this study, the waveguide is made with a width of 10 mm and a penetration length of 7 mm in the pipe cross section, so the effective impact area is 70 mm^2. Since the inner diameter of the test pipeline is 72 mm, the blockage of the waveguide is 1.7% of the pipe cross-sectional area. The rubber bushings embracing the middle section of the waveguide can damp the interfering vibrations of the pipe section [21]. Attached on the outer end of the waveguide is an AE sensor (RS-2A, Softland). The AE sensor converts the elastic stress waves into electrical signals. Since the impact velocity and particle size both affect the elastic stress waves, it is necessary to decouple the effect of the impact velocity on the AE signal in order to infer independent particle size information. Unfortunately, the impact velocity cannot be determined from the AE signal while particle size is unknown and an independent measurement of the impact velocity has to be made. The triboelectric sensing technique is a simple but effective approach to particle velocity measurement [9]. As illustrated in Fig. 2, three identical triboelectric sensor arrays are symmetrically embedded in the pipe wall adjacent to the waveguide. Each triboelectric sensor array has three identical arc-shaped electrodes which are made of stainless steel. The center-to-center spacing between the adjacent electrodes is 20 mm, whilst the axial width of each electrode is 5 mm and the length of each electrode is 36 mm.

For each triboelectric sensor array, the particle velocity is determined by multi-channel correlation of the signals from every pair of the three electrodes and fusion of the three measured velocities. The particle velocity across the entire pipe cross section is derived by fusing the three independent velocities the three sets of triboelectric sensor arrays. The impact velocity required for the on-line particle sizing is the average of the two particle velocities measured from the two sensor arrays (A and C).

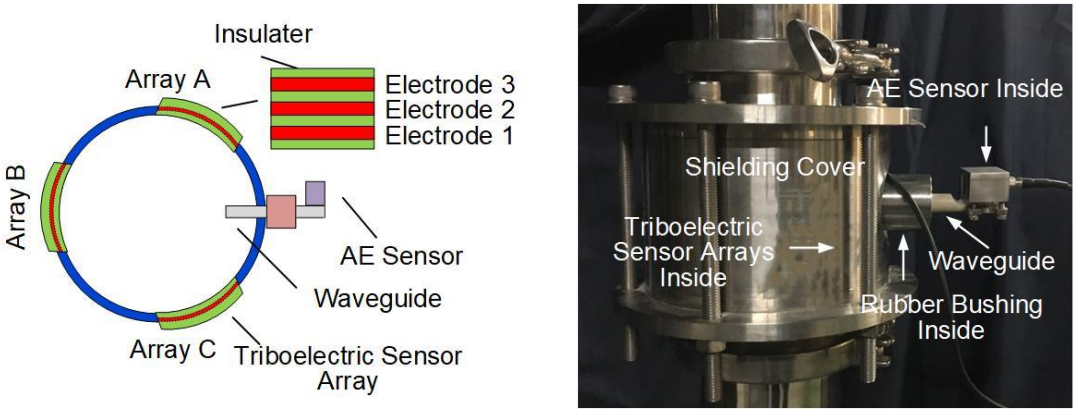

(a) (b)

Fig. 2 Design and installation of the sensing head. (a) Schematic diagram. (b) Photo of the installed sensing head.

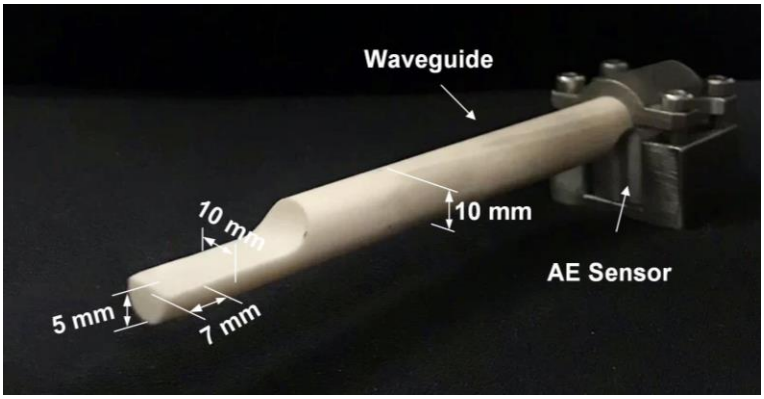

Fig. 3 Photo of the waveguide and AE sensor.

As shown in Fig. 4, the AE and triboelectric signals from the sensing head are connected to a multi-channel signal conditioning unit that performs amplification and filtering. The analog signal from the AE sensor is amplified with a voltage gain of 35 dB and then filtered through a bandpass

filter over a frequency range of 1 kHz – 1 MHz. It should be noted that, since useful particle sizing information may exist in the lower frequency band of 1 kHz to 10 kHz, the lower limit of the band-pass filter is set to 1 kHz instead of 10 kHz (the recommended lower limit by the AE sensor manufacturer). The triboelectric signal from each electrode is converted into a voltage form via an I/V converter, then amplified with a voltage gain of 50 dB and filtered with a cut-off frequency of 2 kHz [9]. With the known impact velocity from the triboelectric sensor arrays, the particle size distribution is derived with the use of a particle sizing algorithm.

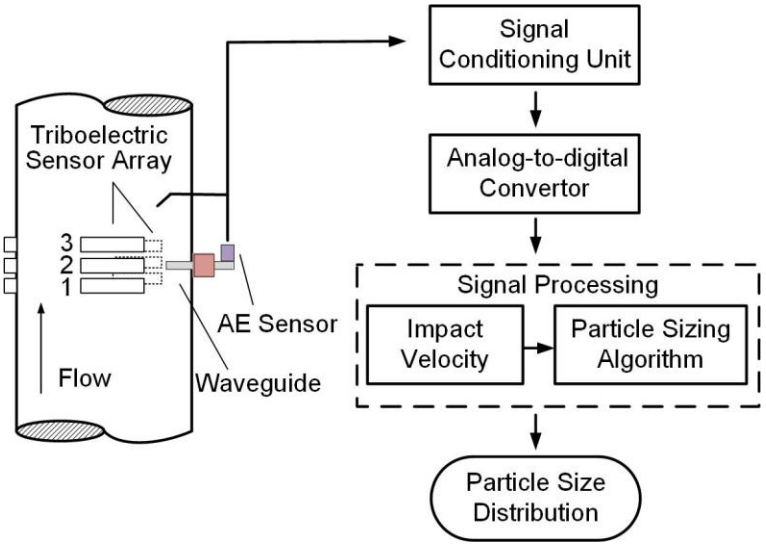

Fig. 4 Principle and structure of the measurement system.

B. Measurement of Particle Impact Velocity

In order to prevent the bounce-back of particles from interfering with the particle impact velocity measurement, the arc-shaped electrodes were not installed in the upstream of the waveguide. Instead, two sets of triboelectric sensor arrays each with three identical arc-shaped electrodes are designed and installed next to the waveguide (Fig. 2). The three-electrode sensing unit has a good reliability on the basis of redundant configuration. By cross-correlating the signals from upstream and downstream electrodes, three independent particle velocities are obtained.

The correlation functions between the three signals are expressed as

$$R_{ij}(\tau) = \frac{1}{T}\int x_i(t)x_j(t+\tau)\,dt \tag{1}$$

where i, j = 1, 2, or 3, $x_i(t)$ and $x_j(t)$ are the signals from upstream and downstream electrodes, respectively, and T is the integration time. The transit time is the time delay for particles to move from the upstream electrode to the downstream electrode, which can be determined by locating the dominant peak of the correlation function. With the known spacing (L_{ij}) between each pair of electrodes and the corresponding transit time (τ_{ij}), the particle velocity measured by each pair of electrodes is calculated from

$$v_{ij} = \frac{L_{ij}}{\tau_{ij}} \tag{2}$$

The local particle velocity of each triboelectric sensor array, v_k, where k is A or B, is determined by fusing the three individual velocities [16]

$$v_k = \frac{r_{12}v_{12} + r_{23}v_{23} + r_{13}v_{13}}{r_{12} + r_{23} + r_{13}} \tag{3}$$

where r_{12}, r_{23} and r_{13} are the amplitudes of the dominant peaks in the cross-correlation functions respectively. As the two identical triboelectric sensor arrays are symmetrically installed adjacent to the waveguide. The particle impact velocity (v) required for the on-line particle sizing is the average of the two local velocities, v_1 and v_2.

C. Particle Sizing Algorithm

Fig. 5 shows the flow chart of the online particle sizing algorithm. The primary peak during each particle impact event is related to the particle size and impact velocity [8]. A peak detection algorithm is used to identify the peak AE voltage. Owing to the simultaneous impact of multiple particles on the waveguide as well as environmental noise, the apparent peak distribution of particle flow obtained from the AE signal deviates from the expected distribution and needs to be

modified. Since particle size distribution in vast majority of practical cases follows the Gaussian distribution, a Gaussian model is thus used to predict peak distribution generated by large and small particles, which can reduce the deviation between the detected peak distribution and expected distribution due to overlapping impacts and environmental noise. With the impact velocity from the triboelectric sensor arrays and the modified peak distribution, the expected particle size distribution is thus obtained by using the impact model. The details of this process are given below.

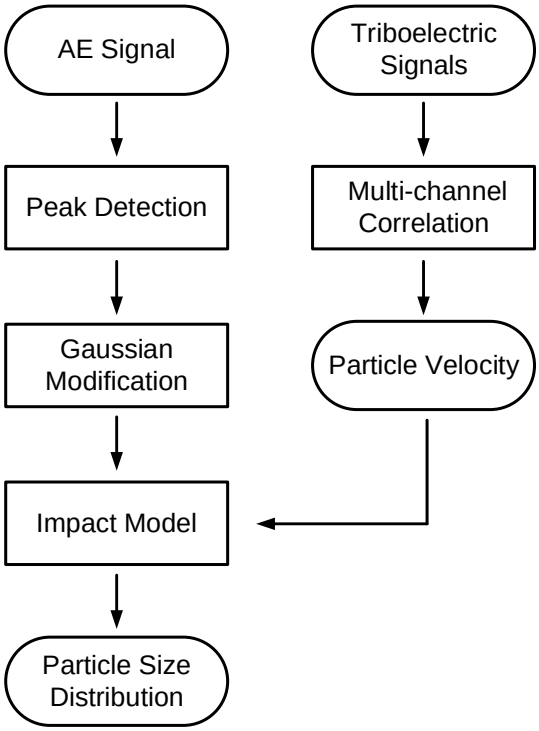

Fig. 5 Flow chart of the particle sizing algorithm.

1) Impact model

The AE signal depends on a sequence of impact events, including the AE source, wave propagation and sensor response. The AE signal can be expressed as [11]

$$V(t)=S(t)*G(t)*D(t) \tag{4}$$

where $V(t)$, $S(t)$, $G(t)$ and $D(t)$ are the functions of the AE signal, acoustic source, wave propagation,

and sensor response, respectively, and t is time. $V(t)$, $S(t)$ and $G(t)$ are also functions of the position where impact takes place. The symbol * represents convolution.

With the Hertz theory of contact [22] and derivation by J. Reed [23], the impulsive force that a spherical particle impacts on an elastic plate can be calculated from

$$S(t)=\begin{cases} F_{max}\left(\sin\left(\dfrac{\pi t}{t_c}\right)\right)^{\frac{3}{2}} & 0<t<t_c \\ 0 & \text{otherwise} \end{cases} \tag{5}$$

where t_c is the contact time and the maximum compression force F_{max} is given by

$$\begin{aligned} F_{max} &= \frac{0.479\rho^{\frac{3}{5}}v^{\frac{6}{5}}d^2}{(\delta_1+\delta_2)^{\frac{2}{5}}} \\ F_{max} &= \frac{0.479\rho^{\frac{3}{5}}}{(\delta_1+\delta_2)^{\frac{2}{5}}} \end{aligned} \tag{6}$$

where ρ, v and d are the mass density, impact velocity and diameter of the spherical particle, respectively. δ_i is a constant depending on the type of material, which is defined by

$$\delta_i = \frac{1-\mu_i^2}{\pi E_i} \tag{7}$$

where i is 1 or 2 and stands for the materials of the particle and plate, respectively. E and μ are Young's modulus and Poisson's ratio, respectively. For the particles of the same material properties, F_{max} is approximated as

$$F_{max} = K_F v^{\frac{6}{5}} d^2 \tag{8}$$

where K_F is a proportionality constant. Eq. (8) indicates that, for a given particle material, the maximum compression force depends only on the impact velocity and particle size.

Since the wave propagation medium and the sensor can be modelled as linear, time invariant

systems, the peak voltage of an AE signal is proportional to the maximum compression force [8], i.e.

$$V_{max} = K_V v^{\frac{6}{5}} d^2 \tag{9}$$

where V_{max} is the peak voltage of the AE signal and K_V is a proportionality constant, which is obtained through calibration with particles to be measured and of known sizes.

The derivation process of Eq. (9) assumes that the particle is spherical, the plate is perfectly flat, and the impact is normal and elastic. However, in practical situations there are many non-ideal factors, including the irregular shape of particles and plastic deformation. In consideration of such non-ideal factors, V_{max} in Eq. (9) should be generalized

$$V_{max} = K_V v^m d^n \tag{10}$$

where indexes *m* and *n* can be obtained through experimental calibration with particles of different size distributions over a range of velocities.

2) Peak detection algorithm

In order to achieve the size distribution measurement of particle flow, the peak voltage of the impact event of each particle should be detected. In this paper, an existing peak detection algorithm based on the local energy is utilized [8]. Fig. 6 shows an example of the procedure, where the small circles represent the identified peaks. Firstly, the local energy for all points is computed and the local energy envelop is smoothed through a mean filter to eliminate some pseudo peaks (Fig. 6(a)). Secondly, the peaks are identified in the energy envelope (Fig. 6(b)). Thirdly, the false peak candidates due to environment noise are removed by applying a certain threshold. Finally, the peak or valley in the AE signal is located by the instant with peak local energy (Fig. 6(c)). Compared to the peak detection algorithms based on time interval [24] or threshold [25], the energy-based peak detection algorithm is more effective in terms of detection success rate.

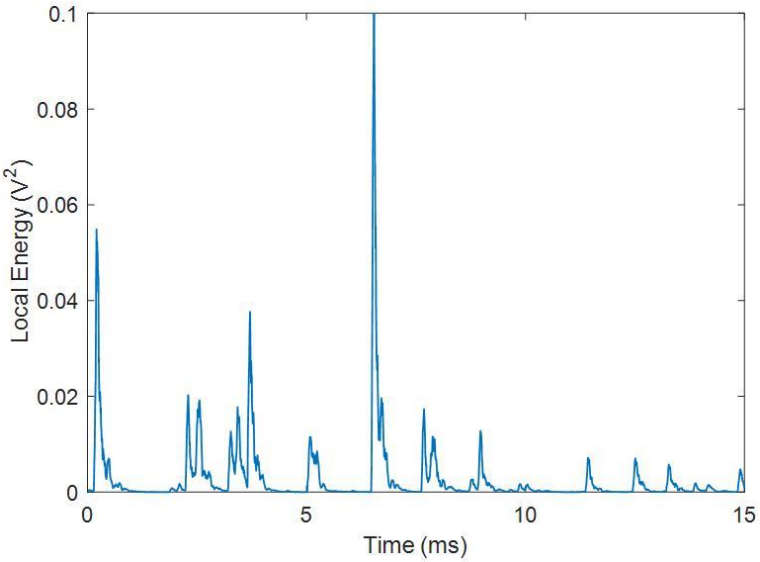
Local Energy (V^2)
0.1
0.08
0.06
0.04
0.02
0
0
5
10
15
Time (ms)

(a)

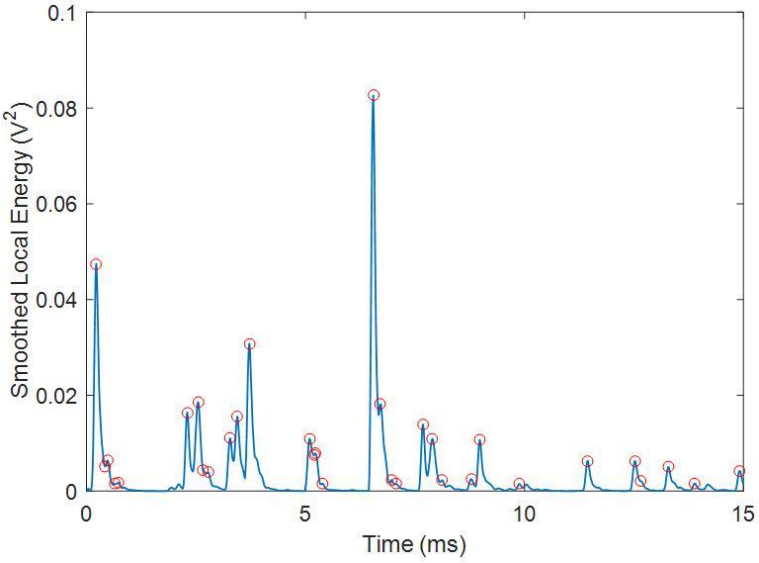
Smoothed Local Energy (V^2)
0.1
0.08
0.06
0.04
0.02
0
0
5
10
15
Time (ms)

(b)

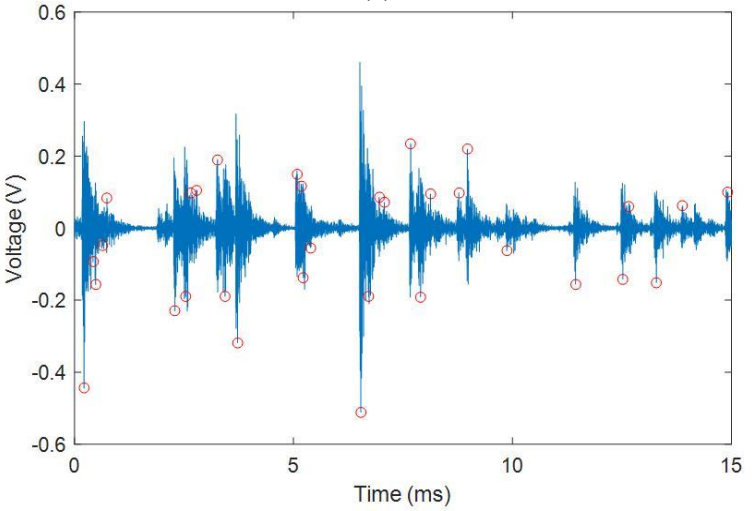
Voltage (V)
0.6
0.4
0.2
0
-0.2
-0.4
-0.6
0
5
10
15
Time (ms)

(c)

Fig. 6 Signal waveforms illustrating the peak detection procedure. (a) Local energy envelope. (b) Smoothed local energy envelope and identified peaks. (c) Identified peaks in the signal.

3) Gaussian prediction

In practical situation some particles hit on the ringing of the previous one or even multiple-particle impact on the waveguide at the same time, resulting in the signal overlapping. For small particles or those with a low impact velocity, the AE pulses are submerged in the background noise and difficult to detect. For such reasons, some of the identified peaks are not valid for on-line particle sizing whilst some impact events may be missed, both affecting the measurement accuracy [8]. Based on the central limit theorem, a large number of particles in the natural state without manual sieving or mixing in a certain ratio usually comply with a Gaussian size distribution [26, 27].

The fit function used to fit the Gaussian model is given by

$$y = ae^{-\frac{(x-b)^2}{2c^2}} \tag{11}$$

where x is a random variable, i.e. the peak in this case, y is the distribution probability of x, i.e. relative frequency, a is the amplitude, b is the distribution center location and c is related to the scale characteristics, i.e. distribution width.

Fig. 7 illustrates the process of Gaussian prediction. The calibration of the Gaussian model is performed on the part of the peak distribution where the peaks are less affected by the aforementioned factors and consistent with the expected distribution. The Gaussian prediction is then applied to the entire peak distribution according to the fitting result. With the impact velocity measured from the triboelectric sensor arrays and determined constant and indexes, the particle size distribution is finally obtained from the modified peak distribution from Eq. (10).

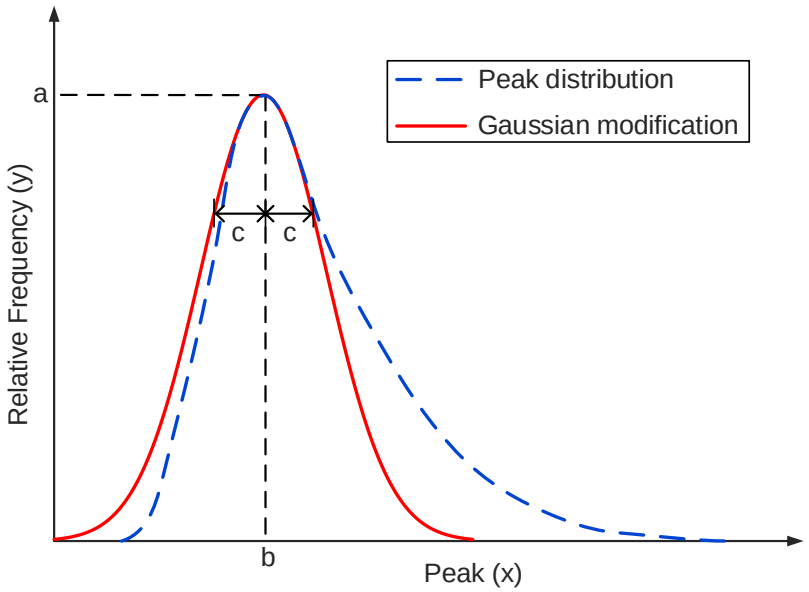

Fig. 7 Illustration of Gaussian prediction.

III. Experimental Results and Discussion

A. Experimental Setup and Material Properties

To evaluate the performance of the prototype particle sizing system, experiments were carried out on a 72 mm bore gas–solids two-phase flow rig. Fig. 8 shows the layout of the test rig. Stable air flow is generated from an industrial suction system connected to the pipeline. Particles are fed into the rig from an adjustable screw feeder at a controlled discharge rate. The sensing head was installed on a vertical section of the stainless steel pipeline.

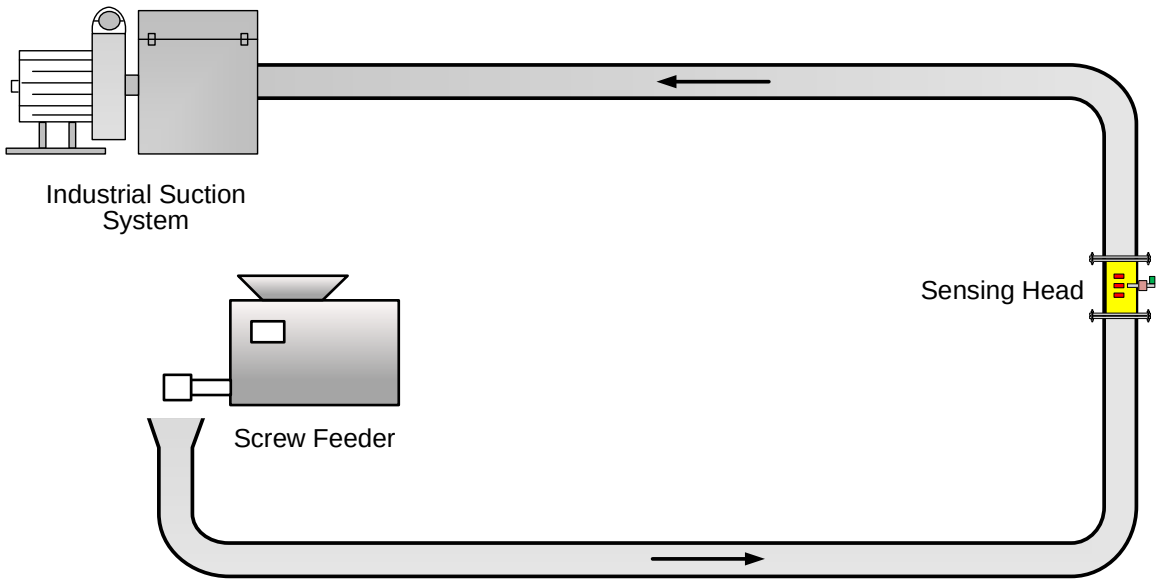

Fig. 8 Layout of the gas–solids two-phase flow rig.

Silica sand is a chemically stable silicate mineral with a density of 2.65 g/cm^3. Since the size, shape and flow characteristics of the pulverized coal and silica sand are similar, silica sand is used as a substitute of pulverized coal for health and safety reasons under laboratory conditions [28, 29]. Fig. 9 shows an image of the test material in this study. The particle shape of the material is irregular (non-spherical). The reference size distribution of the test particles was obtained from a commercial laser particle size analyzer (OMEC LS-POP9), which operates on optical diffraction principles [30]. Fig. 10 depicts the typical size distributions of the three sets of test particles. The smallest set - set III is similar to the particle size at thermal power plants whilst particles in sets II and III are larger because larger particles are a major concern to plant operators as they affect adversely the combustion process in terms of combustion efficiency and emissions [31].

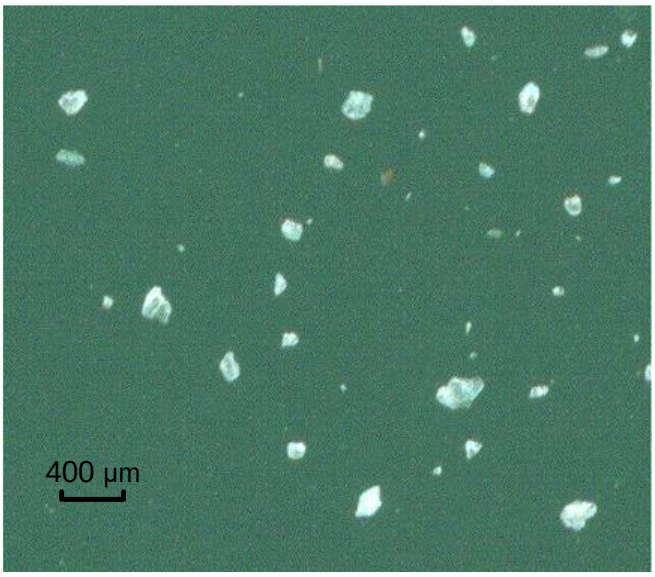

Fig. 9 Typical images of the test particles.

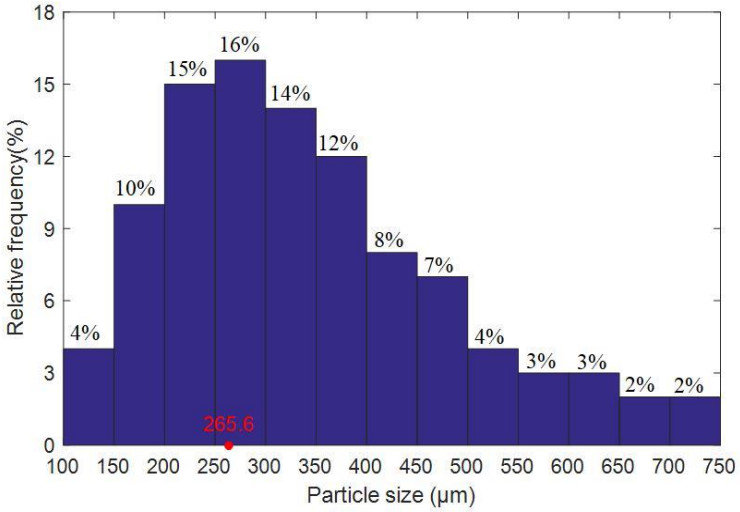

(a)

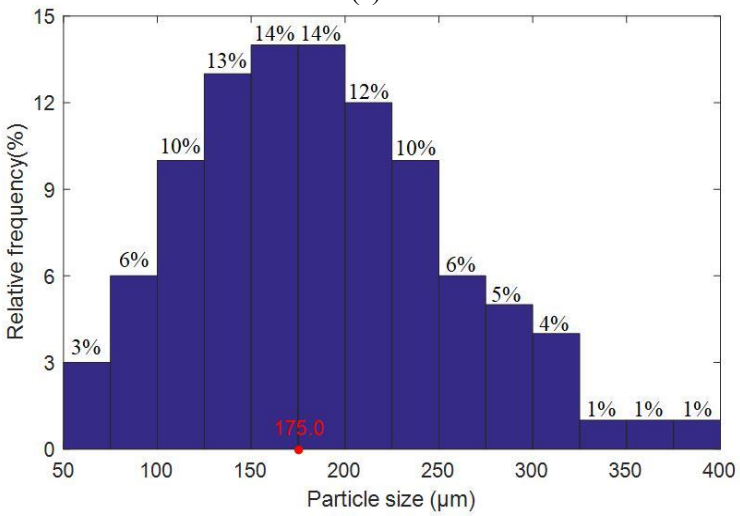

(b)

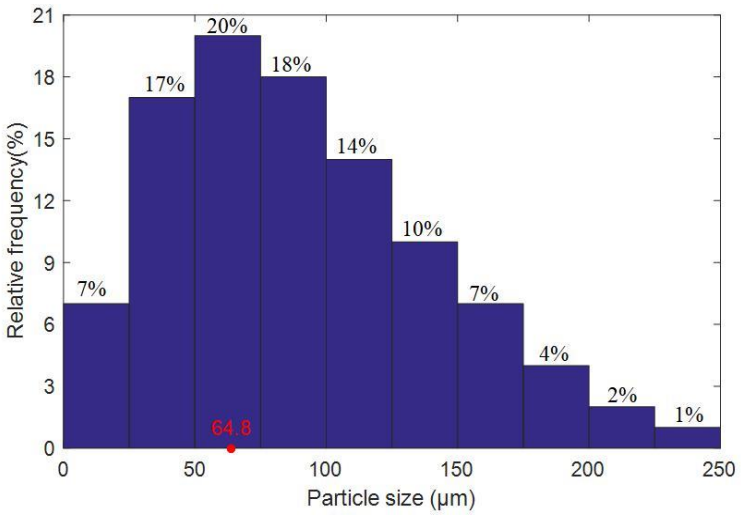

(c)

Fig. 10 Size distributions of the test particles measured from the laser particle size analyzer. (a) Set I. (b) Set II. (c) Set III.

Experiments were carried out under different flow conditions by varying the impact velocity. During the experiment period, the ambient temperature was measured to be between 24.0°C to 26.2°C while the relative humidity ranged from 50% to 53%. Table I summarizes the test conditions along with the size ranges of the test particles. Peak size is the particle size corresponding to the distribution peak, i.e. the highest proportion of particles. The sampling rate of the AE signal is 2 MHz, while the triboelectric signals are sampled at 20 kHz. The window size of data for the triboelectric signals is 1024 data points (51.2 ms). Peak detection is performed on the AE signal every 51.2 ms and the detected peaks are stored. When the sizing system started initially, it takes 8 s to obtain the particle size distribution, which is then refreshed every 51.2 ms. The impact velocity was displayed on the host computer screen in real time. Variations in impact velocity were achieved by changing the power of the industrial suction system (Fig. 8). Each test run lasted for 8 seconds.

TABLE I. EXPERIMENTAL CONDITIONS

Particles	Size range (μm)	Peak size (μm)	Impact velocity (m/s)

Set I	116–750	265.6	21.0, 24.0, 27.0, 30.0
Set II	61–395	175.0	21.0, 24.0, 27.0, 30.0
Set III	10–246	64.8	21.0, 24.0, 27.0, 30.0

B. Results of Particle Impact Velocity Measurement

Fig. 11 plots typical signals from triboelectric sensor array A and resulting correlation functions. As can be seen, the signals from the three electrodes (Fig. 2) are similar with time delays among them. The transit times measured from the correlation functions are 0.85 ms (τ_{12}, electrodes 1&2), 0.81 ms (τ_{23}, electrodes 2&3) and 1.64 ms (τ_{13}, electrodes 1&3), respectively. With the known spacing (L_{12} = L_{23} = 20 mm and L_{13} = 40 mm) between each pair of electrodes, the individual particle velocities are calculated to be 23.61 m/s (v_{12}), 24.58 m/s (v_{23}) and 24.43 m/s (v_{13}), respectively. It is not surprising that there are small discrepancies in the three individual velocities. Factors contributing for these discrepancies include the time-varying nature of the gas-solid two-phase flow, mismatches between the three-channel signal conditioning units, mechanical tolerance in the machining and assembly of the electrodes and insulators. With the known correlation coefficients between electrodes 1&2 (r_{12}= 0,72), 2&3 (r_{23}= 0.72) and 1&3 (r_{13}= 0.49), the local particle velocity from sensor array A is calculated from the individual particle velocities via Eq. (3), which is 24.18 m/s. It is evident that the fusion of the three individual correlation velocities in each sensor array has led to more reliable and repeatable measurement of the local particle velocity.

Fig. 12 presents typical particle velocity measurement results for Set I particles. It is clear that the particle velocity measured from sensor array B is consistently smaller than those from sensor arrays A and C. This result demonstrates that the velocity distribution of particles is indeed

irregular even the sensing head is installed in the vertical section of the pipe. On this particular occasion the difference in the measured local particle velocities is due to the effect of the centrifugal force when particles passed through the lower bend on the test rig (Fig. 8), despite the sensing head was positioned 15 times the pipe diameter away from the lower bend. As the pipe diameter is small and the positions of sensor arrays A and C relative to the elbow are symmetrical, the local particle velocities from sensor arrays A and C are close to each other. In fact, the measured particle impact velocity as shown in Fig. 12 is almost exactly the desired value (Table I).

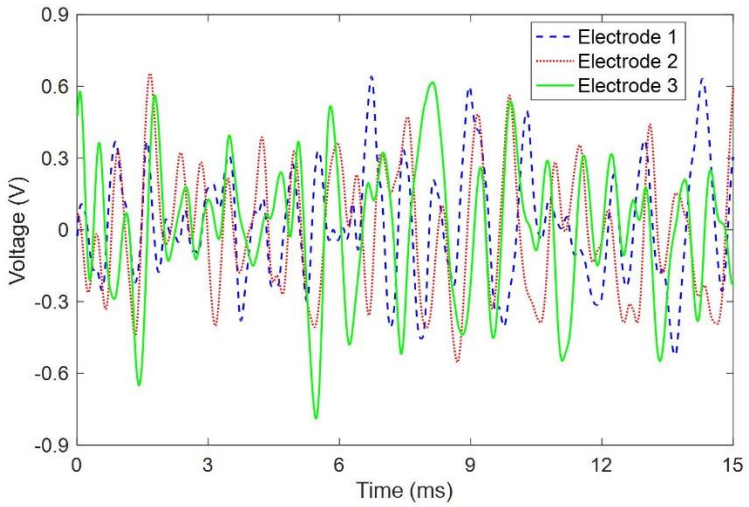

(a)

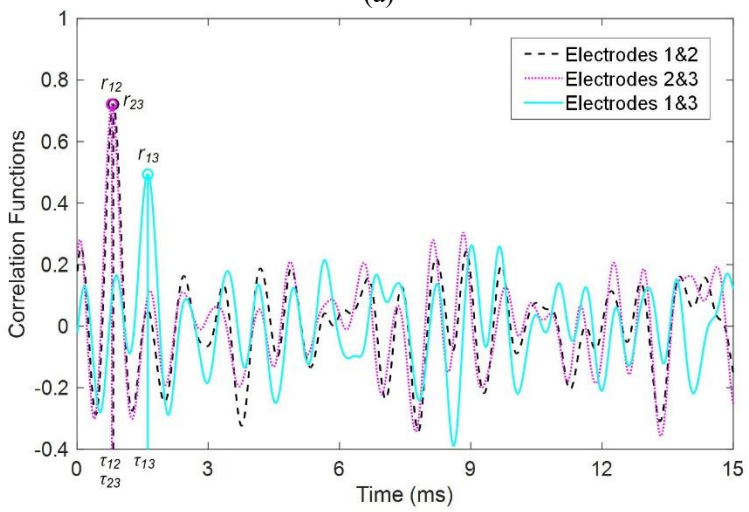

(b)

Fig. 11 Typical triboelectric signals from sensor array A and their corresponding correlation functions. (a) Signals from the three electrodes. (b) Cross-correlation functions.

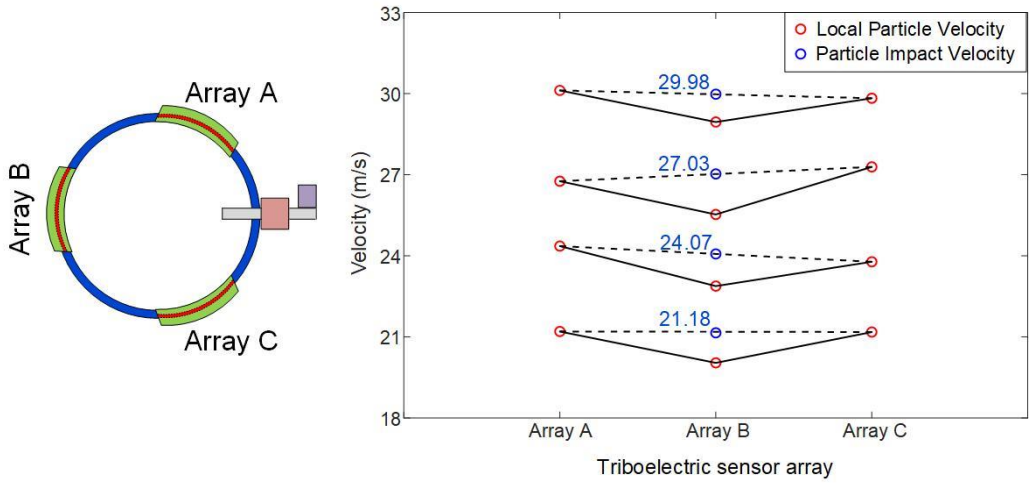

Fig. 12 Measured local particle velocities from the triboelectric sensor arrays and the resulting particle impact velocities (average from arrays A and C).

C. Peak Detection Results

Fig. 13 plots the typical AE signals for the three groups of test particles. As can be seen, most individual impact events can be resolved in the time domain signal, while larger particles generate higher peak voltages. Therefore, the particle sizing algorithm could be partially validated against the individual impact events. The AE signals generated by small particles are difficult to detect because the useful signals are immersed in the strong background noise, which is due mainly to the strong airborne sound from the suction system (Fig. 8). The AE signals with abnormally large peaks originated mostly from concurrent impacts of more than one particles on the waveguide.

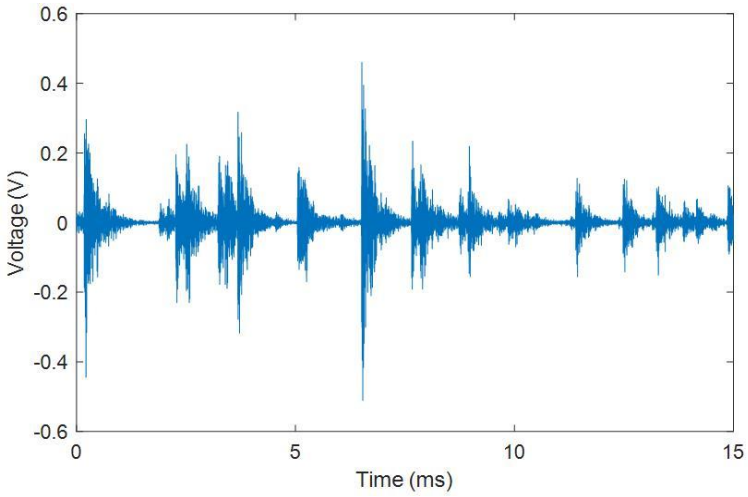

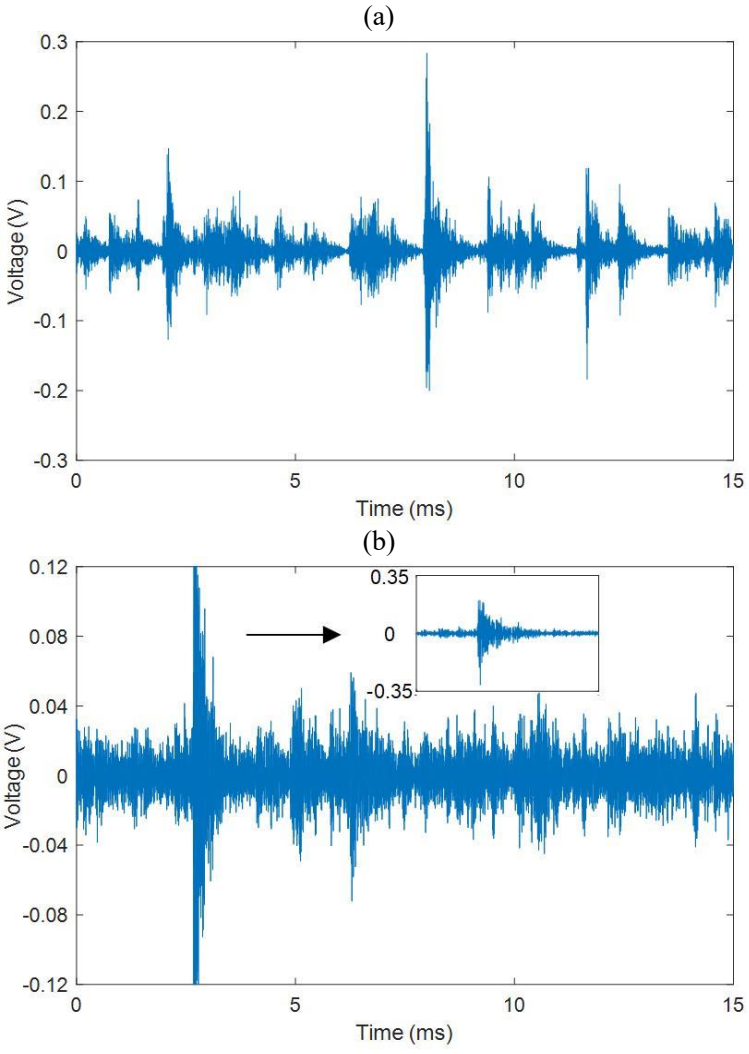

Fig. 13 Typical AE signals at an impact velocity of 30 m/s for different particle size groups. (a) Set I. (b) Set II. (c) Set III.

Fig. 14 shows the peak distribution results at an impact velocity of 30 m/s for different particle size groups. Due to the overlapping of impact events, the number of large peak voltages (left region of the distribution) is unexpectedly large, while the number of small peaks (right region of the distribution) is incorrectly small due to the presence of the environmental noise and the thresholding operation. It is evident from Fig. 14 that the average and median of the peaks are relatively larger than the expected values. The data near the original distribution peak are little affected by the missed detection or overlapping of impact events, so they correspond well with the expected distribution.

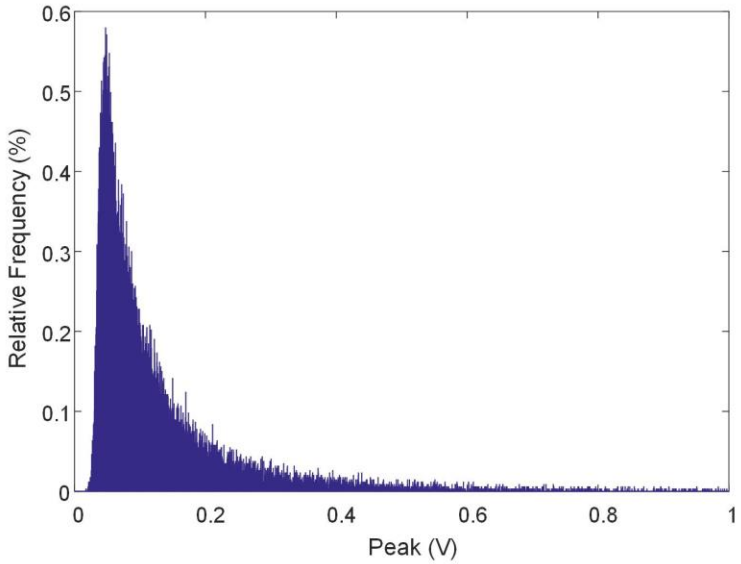
Relative Frequency (%)
0.6
0.5
0.4
0.3
0.2
0.1
0
0
0.2
0.4
0.6
0.8
1
Peak (V)

(a)

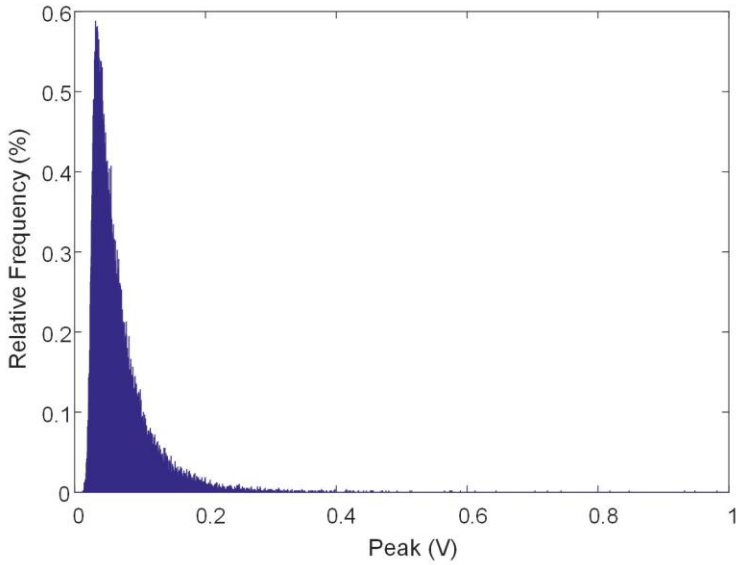
Relative Frequency (%)
0.6
0.5
0.4
0.3
0.2
0.1
0
0
0.2
0.4
0.6
0.8
1
Peak (V)

(b)

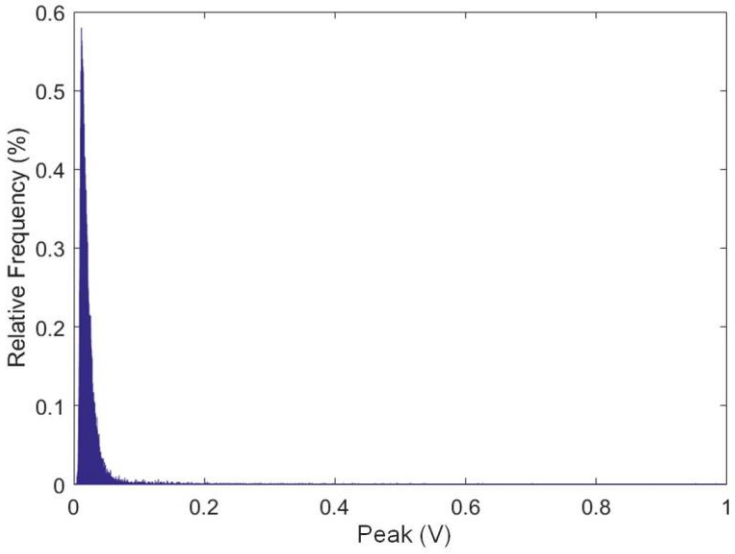

(c)

Fig. 14 Peak distributions at an impact velocity of 30 m/s. (a) Set I. (b) Set II. (c) Set III.

D. Validation of the Impact Model

The peak magnitude increases with both the impact velocity and the particle size. The average values of the peak and impact velocity are used for curve fitting to obtain the index m in Eq. (10). The coefficient of determination R^2 is used to describe the closeness between the measurement data and the curve fitting results. As illustrated in Fig. 15, each set of particles is associated with a curve and a set of m and R^2 are included in the legends. It is clear that there is a good agreement between the fitted curves and measured data points with the R^2 values all greater than 0.9. Meanwhile, the values of m for the three particle groups are almost the same and unaffected by particle size, which agrees with the theoretical analysis. For a fixed impact velocity, the particle size and peak voltage of the AE signal corresponding to the distribution peak can be fitted to a curve to determine the index n in Eq. (10). The fitted curves and the corresponding index n and the R^2 values for four different impact velocities are plotted in Fig. 16. As the R^2 values are all greater than 0.9, the fitted curves are consistent with the measured data. The non-monotonic variations of n suggest that there is no definite relation between n and the impact velocity. Since

the sets of indexes m and n vary only within a narrow range, the average values are used for the determination of the particle size, i.e.

$$V_{\max} = K_V v^{0.98} d^{1.04} \tag{12}$$

The index (0.98) of the impact velocity (m) in Eq. (12) is smaller than that in the analytical model (Eq. (9)). This deviation is believed to be due to plastic deformation and energy loss in the actual impacts between the silica sand particles moving at a velocity greater than 20 m/s and the zirconia ceramic waveguide which is a high-hardness material [11]. Unfortunately, the analytical model (Eq. (9)) is unable to consider the effects of plastic deformation and energy loss during the impact process. Meanwhile, the index (1.04) of particle size (d) in Eq. (12) is significantly smaller than that in the analytical model (Eq. (9)). This is due to the fact that the test particles are of slice type with sharp edges and corners (Fig. 9), which differs considerably from the ideal spherical particles. For a test particle and a spherical particle of the same size (i.e. maximum diameter across the particle), the mass of the former is smaller than that of the latter, leading to a smaller impact force and hence lower AE signal amplitude. Again, such complex factors of irregular particles cannot be incorporated in the analytical modelling (Eq. (9)).

Substituting the peak voltages of AE signals and particle sizes corresponding to the distribution peaks and particle velocities under the above test conditions into Eq. (12) yields

$$V_{\max} = 6.02 v^{0.98} d^{1.04} \tag{13}$$

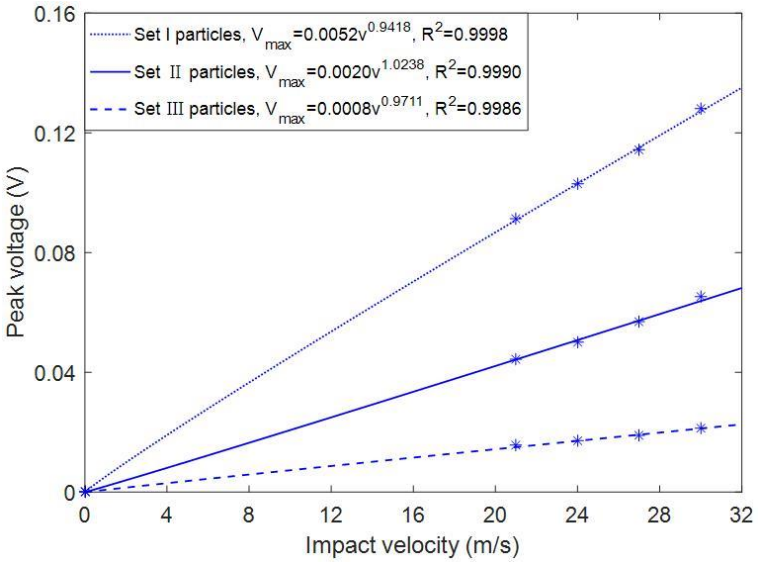

Fig. 15 Relationship between the peak and the impact velocity for three size ranges of particles.

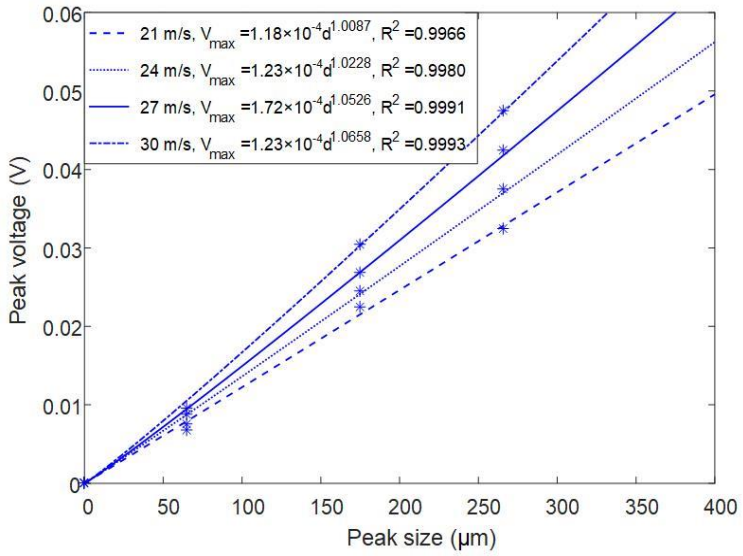

Fig. 16 Relationship between the peak and the particle size for four particle velocities.

E.Measurement Results Through Gaussian Prediction

The Gaussian prediction includes two steps, namely finding the location of the distribution center and the determination of the volume of data used for fitting. As described in Section III.B, the data near the original distribution peak are little affected by the missed detection or overlapping of impact events, so they are used for the determination of the Gaussian model. According to the reference distribution from the laser particle size analyzer, the calibration of the Gaussian model

is performed on the peak distribution obtained under a typical test condition to determine the volume of the distribution data that is required for the determination of the Gaussian model. These distribution data are used to determine the Gaussian model and predict the peak distribution generated by large and small particles.

Fig. 17 shows the peak distribution results and Gaussian approximations of Set I particles. As can be seen, the Gaussian prediction not only reduces significantly the large peaks, thereby minimizing the effect of the overlapping impacts on the results, but also supplements the small peaks that have not been identified. The center location of the Gaussian model is aligned with the peak of the detected peak distribution. According to the trend of the Gaussian prediction, the modified peak distribution is obtained for on-line particle sizing. Fig. 18 is a comparison of the measured particle size distributions before and after Gaussian prediction against the reference distribution. It is evident that the modified particle size distribution agrees well with the original particle size distribution around the distribution peak. The large particle size due to overlapping impact events is eliminated, effectively supplementing other particle size segments in proportion. In this study, Spearman's rank correlation coefficient is used to quantify the similarity between the two distributions [32]. Spearman correlation coefficient is unity when the two distributions are identical and is close to zero when the discrepancy between the two is very large. Over the size range of 0–1800 μm (Fig. 18), Spearman's rank correlation coefficient between the particle size distribution without prediction and the reference distribution is 0.7374, while the coefficient between the modified distribution and the reference distribution is 0.9190.

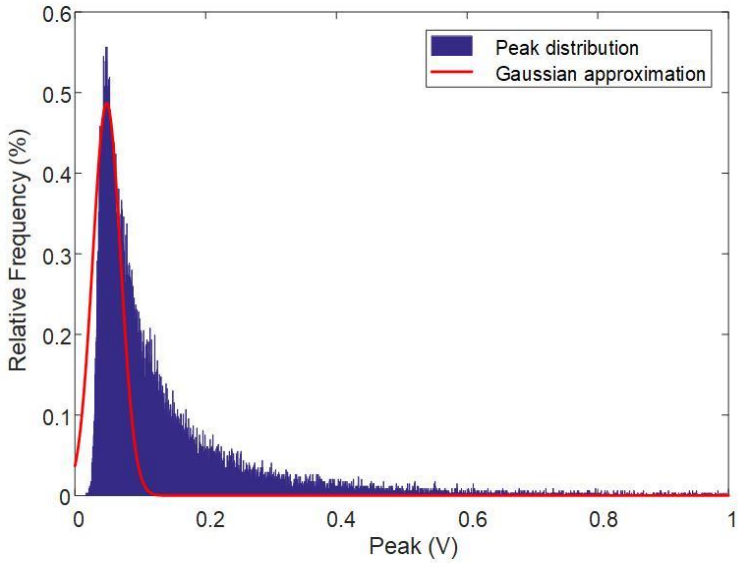

Fig. 17 Peak distribution and Gaussian approximation of Set I particles.

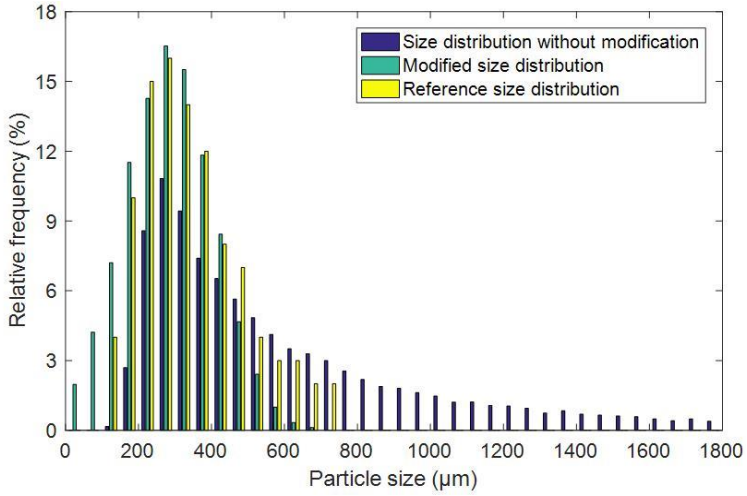

Fig. 18 Measured particle size distribution before and after Gaussian prediction in comparison with the reference distribution.

In term of calibration results, the data with a relative frequency greater than 65% of the distribution peak are used to predict the peak distribution due to the very large or small particles under other test conditions and the results obtained are plotted in Fig. 19. As can be seen, the results at different impact velocities are in good agreement with standard deviation no great than 1%. This small variation in sizing results stems from the natural fluctuations in the impacting particles during each test run. This implies that the on-line particle sizing system has a good repeatability. Fig. 20 shows a direct comparison between the measured and reference particle size distributions

along with the absolute difference between the two for each particle size segment. In this case the relative frequency of each size segment is the average value under all test conditions. Over the size range of 0–750 μm (Fig. 20), Spearman's rank correlation coefficient between the measured and reference particle size distributions is 0.8396. The maximum discrepancy, i.e. the maximum absolute difference between the measured and reference size segments is 4.81% while the average discrepancy of all size segments is 1.73%. This deviation is partly due to the measurement error and partly originates from the natural variations in the particles measured off-line with the laser particle analyzer and those detected on-line in the pneumatic conveying pipeline.

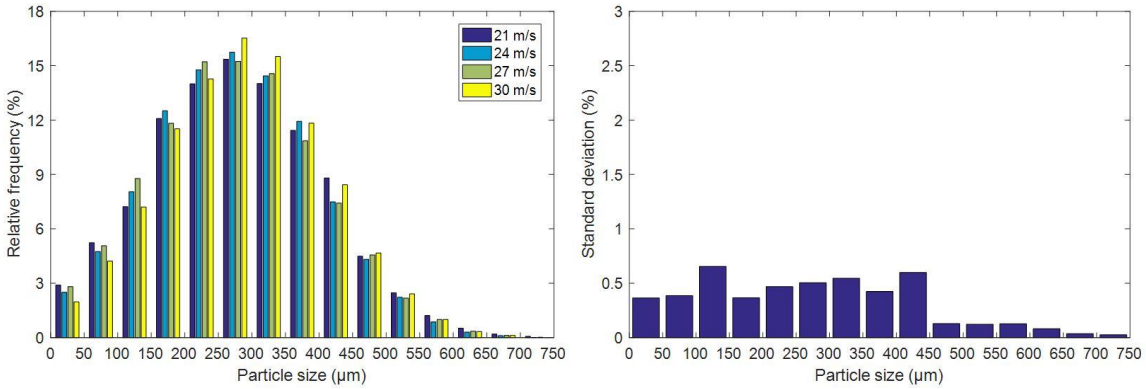

(a) (b)

Fig. 19 Size distribution of Set I particles at different particle velocities. (a) Particle size distribution. (b) Standard deviation of (a).

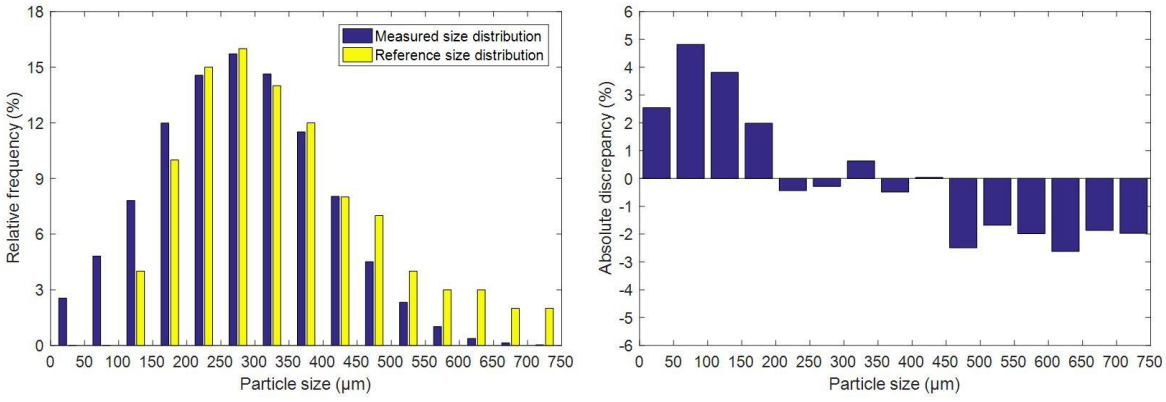

(a) (b)

Fig. 20 The measured and reference size distributions of Set I particles. (a) Particle size distribution. (b) Absolute discrepancy between the measured and reference distributions.

Similarly, the peak distributions of Sets II and III particles are modified with the Gaussian model to predict the peak distribution generated by large and small particles. As shown in Fig. 21 and 22,

the standard deviation of the measurements is no great than 1.5% under all test conditions, which indicates the good similarity between the particle size distributions. Fig. 23 and Fig. 24 illustrate the comparisons of the measured results against the reference distributions. Spearman's rank correlation coefficient between the measured and reference particle size distributions is 0.9513 over the size range of 0–400 μm and 0.9879 over the size range of 0–225 μm, respectively. For Sets II and III particles, the maximum difference between the measured and the reference segments is 2.67% and 3.55%, respectively, while the average discrepancy of all size segments are 1.12% and 2.33%, respectively. However, for materials with particle sizes smaller than Particles III, the overlapping impacts will be more serious due to more simultaneous impacts of particles on the waveguide. When most of the detected peaks are overlapped, the Gaussian prediction will be ineffective, so the measurement results will be much larger than the actual particle size. In this case, the impact area of the waveguide should be reduced significantly, thereby improving the measurement accuracy.

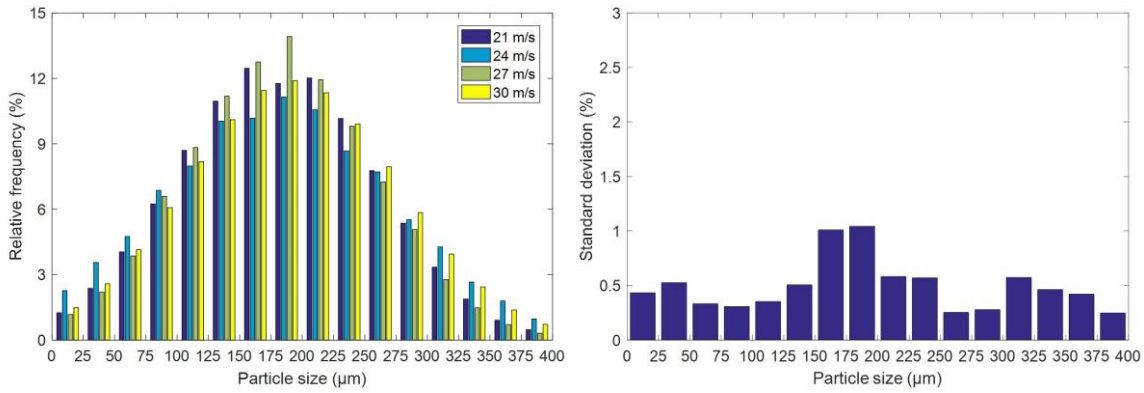

(a) (b)

Fig. 21 Size distribution of Set II particles for different particle velocities. (a) Particle size distribution. (b) Standard deviation of (a).

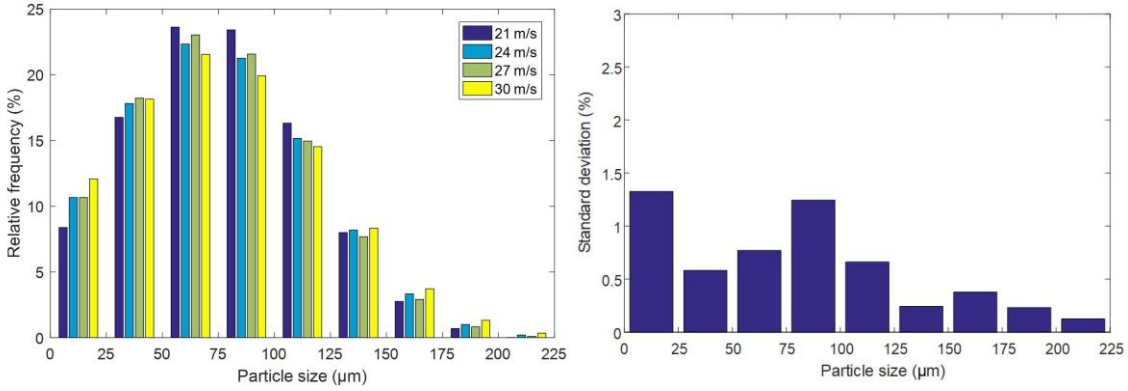

(a) (b)

Fig. 22 Size distribution of Set III particles for different particle velocities. (a) Particle size distribution. (b) Standard deviation of (a).

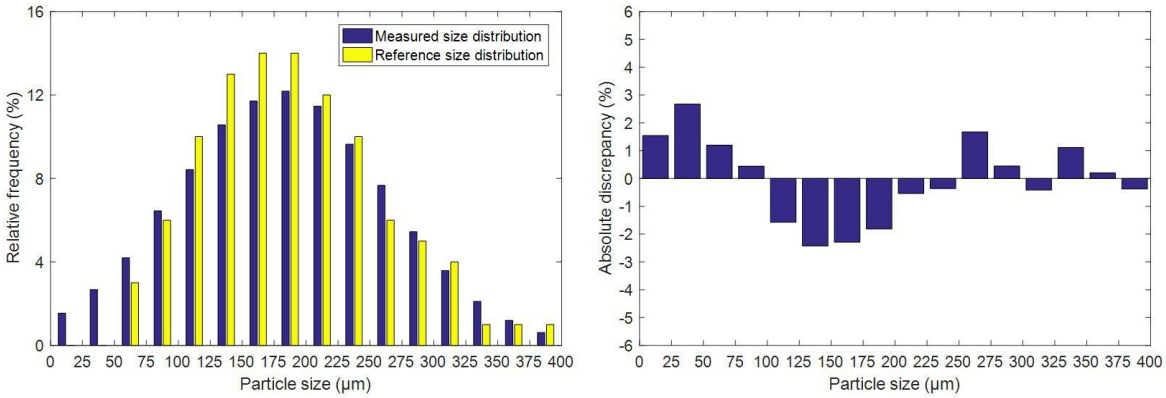

(a) (b)

Fig. 23 Measured and reference size distributions of Set II particles. (a) Particle size distribution. (b) Absolute discrepancy of (a).

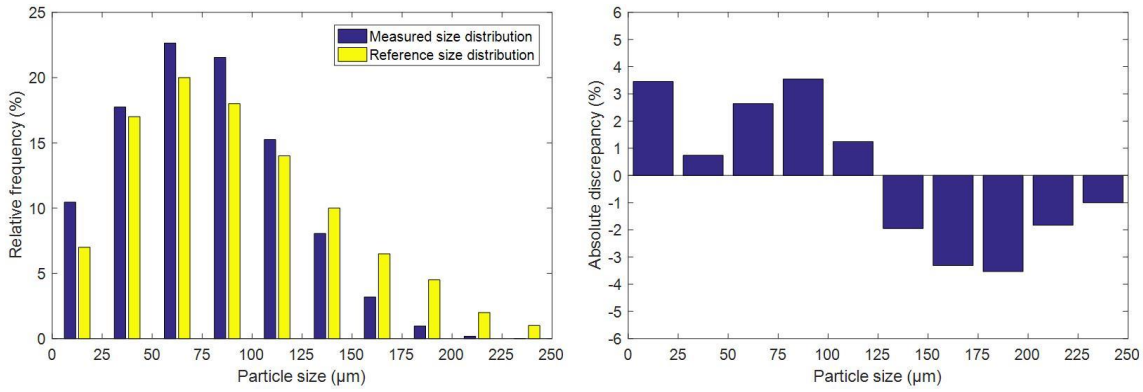

(a) (b)

Fig. 24 Measured and reference size distributions of Set III particles. (a) Particle size distribution. (b) Absolute discrepancy of (a).

IV. CONCLUSIONS

This paper has proposed an instrumentation system using AE detection and triboelectric sensing

techniques for the online measurement of the size distribution of pneumatically conveyed particles. A particle sizing algorithm based on the peak voltage of the AE signal has been developed. The algorithm includes three key elements, peak detection, Gaussian prediction and impact model. Silica sand with three different size ranges, 116–750 μm, 61–395 μm, 10–246 μm, were used as test particles. The experimental results obtained from the prototype instrumentation system have validated the effectiveness of the Gaussian prediction to reduce the deviation between the detected peak distribution and the expected distribution due to overlapping impact events and environmental noise. The results have demonstrated that the measured and reference size distributions agree well with each other with Spearman's rank correlation coefficient greater than 0.8 under all test conditions. For the three sets of test particles of different size ranges, the discrepancy for each particle size segment is within ±4.8%. The results have also indicated that the repeatability of the system is within 1.5% for each particle size segment. It is envisioned that, with the advantages of online continuous measurement, simple structure and cost-effectiveness, the proposed technique should provide an effective solution to the problem of online particle sizing in industry.

ACKNOWLEDGMENT

This work was supported by the National Natural Science Foundation of China under Grant 61573140.

References

[1] R. K. Pan, T. Qiu, J. K. Cha, H. Y. Ma, J. Wang and C. Li, “Thermal evolution of the oxidation characteristics of pulverized coal with different particle sizes and heating rates,” *Thermochim. Acta*, vol. 685, Art. no. 1785162, 2020.

[2] Y. Ninomiya, L. Zhang, A. Sato and Z. Dong, “Influence of coal particle size on particulate matter emission and its chemical species produced during coal combustion,” *Fuel Process. Technol.*, vol. 85, no. 8–10, pp. 1065–1088, 2004.

[3] N. Malumbazo, N. J. Wagner and J. R. Bunt, “The impact of particle size and maceral segregation on char formation in a packed bed combustion unit,” *Fuel*, vol. 111, pp. 350–356, 2013.

[4] X. Cai, J. Li, X. Ouyang, Z. Zhao and M. Su, “In-line measurement of pneumatically conveyed particles by a light transmission fluctuation method,” *Flow Meas. Instrum*., vol. 16, no. 5, pp. 315–320, 2005.

[5] R. M. Carter, Y. Yan and P. Lee, “On-line nonintrusive measurement of particle size distribution through digital imaging,” *IEEE Trans. Instrum. Meas*, vol. 55, pp. 2034–2038, 2006.

[6] T. Tajdari, M. F. Rahmat and N. A. Wahab, “New technique to measure particle size using electrostatic sensor,” *J. Electrostat.*, vol. 72, no. 2, pp. 120–128, 2014.

[7] Y. Shirakawa, Y. Matsuo, J. Ohno, S. Watanabe and H. Yashiro, “On-line measurement of particle size by microwave technology,” *Nippon Steel, Tech. Rep.*, no. 49, pp. 9–14, 1991.

[8] Y. Hu, L. Wang, X. Huang X. Qian, L. Gao and Y. Yan, “On-line sizing of pneumatically conveyed particles through acoustic emission detection and signal analysis,” *IEEE Trans. Instrum. Meas.*, vol. 64, no. 5, pp.1100–1109, 2015.

[9] Y. Yan, Y. Hu, L. Wang, X. Qian, W. Zhang, K. Reda, J. Wu and G. Zheng, "Electrostatic sensors – their principles and applications," *Measurement*, vol. 169, Art. no. 108506, 2021.

[10] Y. Yan, "Mass flow measurement of bulk solids in pneumatic pipelines," *Meas. Sci. Technol.*, vol. 7, no. 12, pp. 1687–1706, 1996.

[11] D. J. Buttle, S. R. Martin and C. B. Scruby, "Particle sizing by quantitative acoustic emission," *Res. Nondestruct. Eval.* vol. 3, pp. 1–26, 1991.

[12] M. G. Droubi, R. L. Reuben and G. White, "Monitoring acoustic emission (AE) energy in slurry impingement using a new model for particle impact,". *Mech. Syst. Signal Proc.*, vol. 62–63, pp. 415–430, 2015.

[13] P. J. Coghill, "Particle size of pneumatically conveyed powders measured using impact duration," *Part. Part. Syst. Charact.*, vol. 24, pp. 464–469, 2007.

[14] M. Uher and P. Beneš, "Measurement of particle size distribution by the use of acoustic emission method," in *IEEE International Instrumentation and Measurement Technology Conference*, Graz, Austria, May 13–16, 2012, pp. 1194–1198.

[15] G. Zhang, Y. Yan, Y. Hu, and G. Zheng, "On-line size measurement of pneumatically conveyed particles through acoustic emission sensing," *Powder Technol.*, vol. 353, pp. 195–201, 2019.

[16] X. Qian, Y. Yan, X. Huang and Y. Hu, "Measurement of the mass flow and velocity distributions of pulverized fuel in primary air pipes using electrostatic sensing techniques," *IEEE Trans. Meas. Instrum.*, vol. 66, no. 5, pp. 944–952, 2017.

[17] N. C. Hii, C. K. Tan, S. J. Wilcox, and Z. S. Chong. "An investigation of the generation of acoustic emission from the flow of particulate solids in pipelines," *Powder Technol.*, vol. 243, pp. 120–129, 2013.

[18] Y. Yan, B. Byrne, S. Woodhead and J. Coulthard, “Velocity measurement of pneumatically conveyed solids using electrodynamic sensors,” *Meas. Sci. Technol.*, vol. 6, no. 5, pp. 515–537, 1995.

[19] J. An, Z. Wang, T. Jiang, P. Chen, X. Liang, J. Shao, J. Nie, M. Xu and Z. Wang, "Reliable mechatronic indicator for self-powered liquid sensing toward smart manufacture and safe transportation," *Mater. Today*, vol. 41, pp. 10-20, 2020.

[20] W. Zhang, L. Deng, L. Yang, P. Yang, D. Diao, P. Wang and Z. Wang, "Multilanguage-handwriting self-powered recognition based on triboelectric nanogenerator enabled machine learning," *Nano Energy*, vol. 77, Art. no. 105174, 2020.

[21] G. Zheng, Y. Yan, Y. Hu, W. Zhang, L. Yang and L. Li, “Mass flow rate measurement of pneumatically conveyed particles through acoustic emission detection and electrostatic sensing,” *IEEE Trans. Instrum. Meas.*, in press, 2020.

[22] J. Stronge, *Impact Mechanics.* Cambridge, UK: Cambridge University Press, 2004.

[23] J. Reed, “Energy losses due to elastic wave propagation during an elastic impact,” *J. Phys. D. Appl. Phys.*, vol. 18, pp. 2329–2337, 1985.

[24] B. Dhont, G. Rousseau and C. Ancey, “Continuous monitoring of bed-load transport in a laboratory flume using an impact sensor,” *J. Hydraul.Eng.*, vol. 143, no. 6, Art. no. 04017005, 2017.

[25] V. Ivantsiv, J. K. Spelt and M. Papini, “Mass flow rate measurement in abrasive jets using acoustic emission,” *Meas. Sci. Technol.*, vol. 20, Art. no. 095402, 2009.

[26] C. Pecorari, “Characterizing particle flow by acoustic emission,” *J. Nondestruct. Eval.*, vol. 32, no. 1, pp. 104–111, 2013.

[27] M. F. Leach, G. A. Rubin and J. C. Williams, “Analysis of gaussian size distribution of rigid particles from their acoustic emission,” *Powder Technol.*, vol. 19, no. 2, pp. 189–195, 1978.

[28] W. Zhang, C. Wang and H. Wang, "Hilbert–Huang transform-based electrostatic signal analysis of ring-Shape electrodes with different widths," *IEEE Trans. Instrum. Meas.*, vol. 61, no. 5, pp. 1209–1277, 2012.

[29] C. Wang, H. Yu, N. Zhan, X. Kang and J. Zhang, "A vibration probe sensor for mass flow rate measurement of gas-solid two-phase flow," *Sens. Rev.*, vol. 36, no.2, pp. 200–206, 2016.

[30] C. Jedari; A. Palomino, E. Drumm, H. Cyr, “Comparison of hydrometer analysis and laser diffraction method for measuring particle and floc size distribution applied to fine coal refuse,” *Geotech. Test. J.*, vol. 43, no. 6, pp. 1418–1435, 2020.

[31] Y. Fukayama, K. Hirasawa, K. Shimohira and H. Kanemoto, "An adaptive State estimator for pulverizer control using moments of particle size distribution," *IEEE Trans. Control Syst. Technol.*, vol. 12, no. 6, pp. 797–810, 2004.

[32] G Frapporti, L.A.M Linnartz, and S.P Vriend, “Spearman Base program for computation and testing of Spearman rank correlation coefficient distributions,” *Comput. Geosci.*, vol. 17, no. 4. pp. 569–589, 1991.